How to cite: *Angew. Chem. Int. Ed.* **2021**, *60*, 18472–18477
International Edition: doi.org/10.1002/anie.202105401
German Edition: doi.org/10.1002/ange.202105401

Cyclophanes | Hot Paper

Neutral Unsymmetrical Coordinated Cyclophane Polymerization Catalysts

Eva Schiebel[+], Maria Voccia[+], Laura Falivene, Inigo Göttker-Schnetmann, Lucia Caporaso, and Stefan Mecking**

Abstract: *Cyclophane structures can control steric pressure in the otherwise open spaces of square-planar d^8-metal catalysts. This elegant concept was so far limited to symmetrical coordinated metals. We report how a cyclophane motif can be generated in ligands that chelate via two different donors. An ancillary second imine in the versatile κ^2-N,O-salicylaldiminato catalyst type enables ring closure via olefin metathesis and selective double bond hydrogenation to yield a 30-membered ring efficiently. Experimental and theoretical analyses show the ancillary imine is directed away from the active site and inert for catalysis. In ethylene polymerization the cyclophane catalyst is more active and temperature stable vs. an open structure reference, notably also in polar solvents. Increased molecular weights and decreased degrees of branching can be traced to an increased energy of sterically demanding transition states by the encircling cyclophane while chain propagation remains highly efficient.*

The steric environment of a catalytically active site experienced by the substrates is key to determine favorable reaction pathways. Square planar coordinated active sites, as encountered in innumerable d^8-metal catalysts, are particularly challenging in this regard due to the relatively low coordination number and the consequently large open spaces in the apical direction. A prominent example are late transition metal olefin polymerization catalysts.[1] Compared to traditional d^0-metal catalysts,[2] the less electron deficient and less oxophilic nature of such d^8-metal sites results in functional group tolerance. At the same time, the propensity for ß-H elimination (BHE) enables the formation of unique branching structures,[3] but the BHE pathway also needs to be controlled as it determines not only the branching microstructure but also the polymer molecular weights. A sophisticated approach to generate a defined rigid environment also in those spatial positions remote to the coordination plane and to the donor atoms of square-planar coordinated catalysts is provided by cyclophanes. Guan et al. devised an elegant strategy to generate two alkane bridges between the two identical *N*-terphenyl groups of an α-diimine catalyst (Figure 1).[4–8] The effective blocking of the axial sites enhanced the control of molecular weight in ethylene polymerization as well as temperature stability of the catalysts. However, this approach is restricted to symmetrically coordinated catalysts.

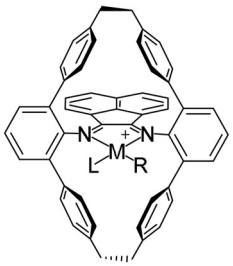

M = Ni, Pd

Figure 1. Cyclophane structure in symmetrical κ^2-*N,N*-coordinated cationic catalysts.

Means to introduce cyclophane motifs also to unsymmetrical coordinated catalysts with different types of donors are desirable. This can unlock a large diversity of possible structures in principle, which can provide unique properties. For example, polymerization catalysts with an unsymmetrical κ^2-*N,O*-chelate are known to stand out in their tolerance towards polar reaction media.[9,10]

We now show how a cyclophane motif can be generated in an unsymmetrically coordinated catalyst, and reveal how the cyclophane environment impacts reaction pathways in ethylene polymerization.

The ring closure as a key step was possible by olefin metathesis in the generation of Guan's α-diimine cyclophane complexes (Figure 1), bridging the terphenyl groups on the two *N*-donors.[4–8] In order to exploit this elegant and proven ring closing chemistry to the problem of unsymmetrically coordinated complexes, we introduced a second catalytically inert (vide infra) imine function on the salicyl ring of κ^2-*N,O*-coordinated Ni^{II} salicylaldiminato complexes.[11,12] Targeting a structure amenable to ring closing, terphenyl anilines with an allyl group on the distal aryl rings were synthesized (Scheme 1).

An additional 3,5-dimethyl substitution pattern was employed on these rings, as this has been found to provide a sensitive probe for their impact on catalysis.[13] Despite the stronger steric hindrance in the 2-position, the higher transmetalation reactivity of the iodide enabled selective copper-assisted cross-coupling[14] of 5-bromo-1,3-dimethyl-2-iodobenzene with allyl bromide to give **1**, with an intact aryl-

[*] E. Schiebel,[+] Dr. I. Göttker-Schnetmann, Prof. Dr. S. Mecking
Chair of Chemical Materials Science, Department of Chemistry, University of Konstanz
Universitätsstraße 10, 78457 Konstanz (Germany)
E-mail: stefan.mecking@uni-konstanz.de
M. Voccia,[+] Dr. L. Falivene, Prof. Dr. L. Caporaso
Dipartimento di Chimica e Biologia, Università di Salerno
Via Papa Paolo Giovanni II, 84084 Fisciano (Italy)
E-mail: lcaporaso@unisa.it
[+] These authors contributed equally to this work.
Supporting information and the ORCID identification number(s) for the author(s) of this article can be found under: https://doi.org/10.1002/anie.202105401.

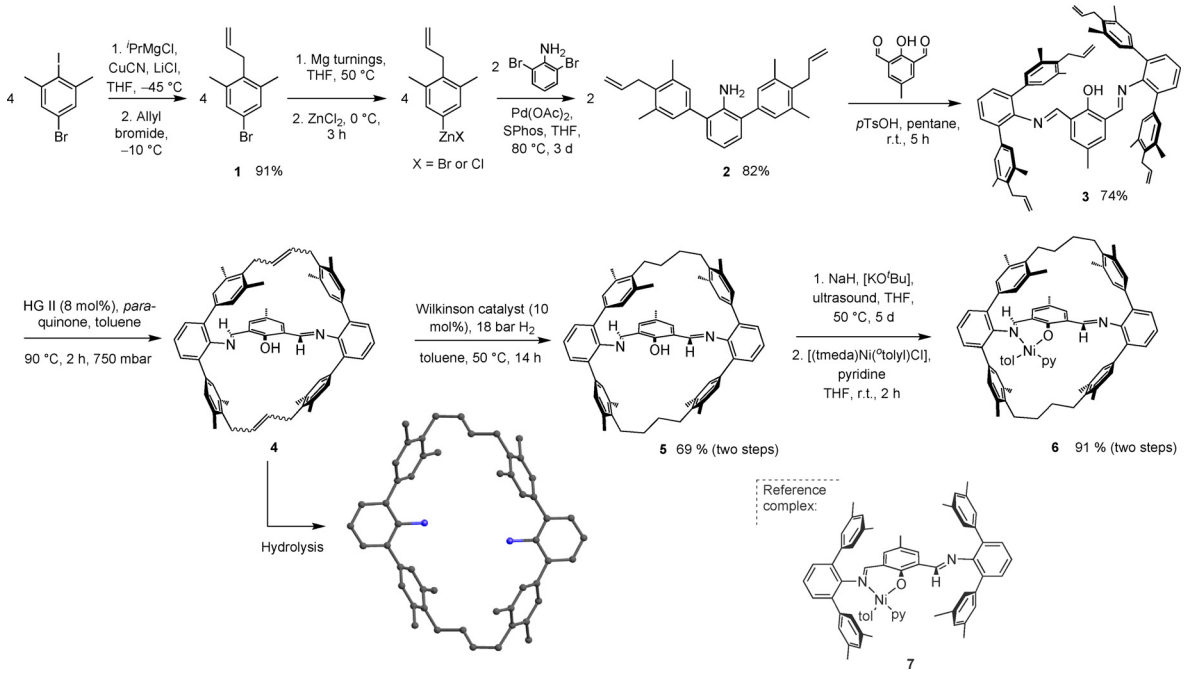

Scheme 1. Synthesis scheme for an *N*,*O*-coordinated Ni^{II} phenoxydiimine cyclophane complex (**6**). The solid-state structure of a hydrolysis product of **4**[15] is also shown, and a non-bridged reference complex (**7**).

bromide (cf. the Supporting Information, for experimental details and characterization data of all compounds). Conversion via a Grignard reaction to the zinc organyl and its Negishi coupling with 2,6-dibromoaniline in THF solution afforded the terphenyl **2**. Condensation with 2,6-diformyl-4-methyl-phenol yielded the bis(imino)phenol **3**, after precipitation from methanol. The key ring closing step proceeds via two intramolecular olefin metathesis reactions, to form three interconnected up to 30-membered rings. Careful optimization showed that high conversions and a high preference for intramolecular reactions could be achieved with Hoveyda–Grubbs II catalyst, at a high reaction temperature of 90 °C that enables rapid activation of the metathesis catalyst, a limited concentration of the substrate (1 $g\,L^{-1}$, in toluene), and a slightly reduced pressure of $p = 750$ mbar to facilitate removal of ethylene as well as a short reaction time of $t = 2$ h. The identity of the product (**4**) was established by NMR techniques and mass spectrometry (cf. Supporting Information) and further confirmed by single crystal X-ray diffraction of a hydrolysis product, (Scheme 1, and Supporting Information). **4** is highly sensitive towards hydrolysis and can be used as received in the hydrogenation step, avoiding intermediate handling in purification steps. Selective double bond hydrogenation without hydrogenation of the imine moieties (and subsequent hydrogenolysis of the formed *N*-benzyls)[16] was achieved with Wilkinson's catalyst at a hydrogen pressure of 20 bar. Purification by column chromatography under dry conditions afforded **5** in an overall yield of 69 % over these two key steps. Surprisingly, the phenol **5** did not react with [(tmeda)$NiMe_2$],[17] even under forcing reaction conditions. The alternative salt metathesis[10,11,18] required a deprotonation of the sterically shielded phenolic proton of **5**. A complete deprotonation was possible by reaction with sodium hydride and catalytic amounts of potassium *tert*-butoxide in THF at 50 °C. Reaction of this sodium salt with [(tmeda)Ni(*o*tolyl)Cl] in the presence of pyridine yielded the desired complex **6**. A non-bridged reference complex (**7**) was prepared for comparison (for experimental details, see Supporting Information).

The target complex **6** was fully characterized by NMR techniques (^1H NMR, ^{13}C NMR, $^1H^1H$ COSY, $^1H^{13}C$ HSQC, $^1H^{13}C$ HMBC). The non-coordinating imine function is rotated away from the nickel atom, which is evident from the imine-C<u>H</u> chemical shift. For the free protonated bis-(imino)phenol, the two imine groups give rise to a single resonance ($\delta = 7.38$ ppm). Upon metal coordination, the proton of the imine coordinating to the metal is more shielded ($\delta = 7.20$ ppm), whereas the non-coordinated imine-C<u>H</u> proton is deshielded due to an interaction with the oxygen atom ($\delta = 7.73$ ppm). The observation of six distinct ^1H and ^{13}C aryl-<u>Me</u> resonances show that the terphenyl groups of the cyclophane complex do not rotate on NMR timescales, as their movement is restricted through the C4 alkane bridges (see conformational analysis, Supporting Information).

The solid-state structures of **6** (Figure 2) obtained by single crystal X-ray diffraction further confirms its identity and conformation. In detail, the nickel atom is oriented almost perfectly square planar, with a very low deviation from the center of the plane ($d(Ni\text{-}plane_{NONC}\text{-}center) = 0.0766(11)$ Å, compared to $d(Ni\text{-}plane_{NONC}\text{-}center) = 0.086(3)$ Å for **7**), and only a slight deviation from 90° angles (angles: N_{imine}-Ni-O: 92.8(2)°, vs. 94.01(9)° found for **7**).

The non-coordinated imine arm is rotated away for both complexes, which releases steric pressure and benefits from the interaction of the imine–C<u>H</u> and the oxygen atom. The

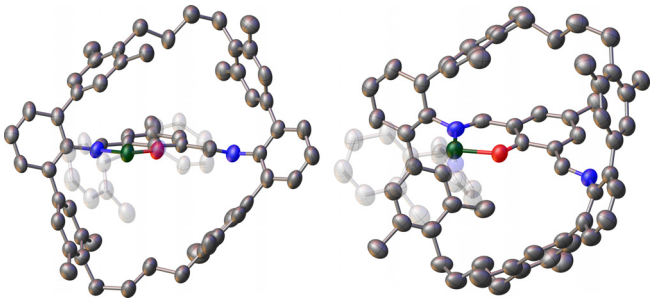

Figure 2. Solid-state structure of **6** from two different perspectives. The ellipsoids are drawn at a 30% probability level, hydrogens are omitted, and the initiating Ni-aryl group and the pyridine are drawn translucent.[15]

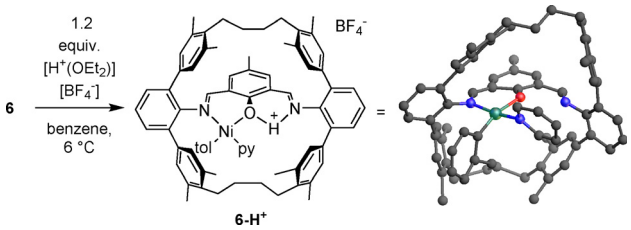

Scheme 2. Synthesis and solid-state structure (obtained from single crystal analysis, counter-ion and hydrogens omitted for clarity) of **6-H$^+$**.[15]

O···H distance ($d_{H-O}=2.546(2)$ Å for **4**, $d_{H-O}=2.437(4)$ Å for **7**) is lower than the sum of the van der Waals radii ($\Sigma_{vdW}=2.72$ Å).[19] This preferred orientation of the non-coordinated imine was confirmed by theoretical calculations, where the isomer with the imine rotated away is lower in energy for all intermediates and transition states (vide infra).

To probe for the flexibility of the cyclophane ligand and potentially overcome the imine's N=C–H···O interaction, the neutral cyclophane complex was protonated (Scheme 2). The solid-state structure of the product, indeed, showed that the second imine group can rotate to form a *N,O*-chelate for the incoming proton despite the C_4 bridges, which shows that the cyclophane ligand also allows for adopting this geometry in principle.

In pressure reactor polymerization experiments (Table 1), the cyclophane catalyst is found to be considerably more temperature stable than the reference (**7**). The productivity, represented by the turnover number (TON), is increased for the cyclophane system. As expected, BHE increases with reaction temperature as indicated by increased branching densities and decreased molecular weight (entries 1 to 3). For all temperatures, branching density of the products are significantly lower compared to the reference catalyst, which produced hyperbranched oligomers (95 branches per 1000 C atoms by $^{13}C\{^1H\}$ NMR, $M_n \approx 1.0$ kg mol^{-1}, by ^1H NMR) when activated (requiring $T \geq 50$ °C). Note that the products of the reference catalyst do not differ from products formed with mono(imino)phenoxy catalysts,[20] underlining the inert nature of the second imine function. Copolymerization with norbornene as a reactive, but bulky substrate was studied to further probe the properties of the catalyst from **6**. Norbornene is incorporated easily with Ni^{II} salicylaldiminato catalysts, with an only two- to threefold higher reactivity of ethylene (e.g. an incorporation of $x_{NB,polymer}=4.6$ mol% at a mole fraction in the reaction mixture of 14%).[21] By contrast, **6** incorporated just $x_{NB,polymer}=0.26$ mol%. This underlines a more sterically congested nature of the active site. Notably, **6** is tolerant towards polar reaction media as exemplified by polymerizations in THF as well as 2-Me-THF, a popular alternative polar solvent accessible from lignocellulose feedstock (Table 1, entries 7–14). Again the cyclophane catalyst is significantly more productive vs. reference **7**, as a result of a higher catalyst stability and faster activation (see Figur-

Table 1: Ethylene polymerizations with **6** and **7**.

#	precatalyst	solvent	T [°C]	n_{precat} [µmol]	t [h]	yield [g]	productivity [TON][b]	M_n (NMR) [kg mol^{-1}][c]	M_n (GPC) [kg mol^{-1}]	M_w/M_n	B[f,g]	% Me[g]
1	**6**	toluene	30	5	7.0	6.3	4.5	1.8	5.8[d]	4.4[d]	26	99
2	**6**	toluene	50	10	1.0	4.0	1.4	1.7	1.9[d]	4.4[d]	48	94
3	**6**	toluene	70	5	1.0	2.9	2.1	1.1	1.5[d]	3.0[d]	61	92
4	**7**	toluene	30	5	2.0	–[a]	–[a]	–[a]	–[a]	–[a]	–[a]	–[a]
5	**7**	toluene	50	5	1.0	0.6	0.4	1.3	1.1[d]	1.9[d]	97	82
6	**7**	toluene	70	5	1.0	0.7	0.5	1.0	1.1[d]	1.9[d]	95	75
7	**6**	THF	50	10	2.25[h]	8.23	2.9	1.2	2.1[d]	8.1[d]	58	95
8	**6**	THF	70	10	1.75[h]	6.73	2.4	1.1	1.5[d]	3.4[d]	75	91
9	**7**	THF	50	10	1.5[h]	4.31	1.5	1.0	2.1[e]	1.8[e]	88	75
10	**7**	THF	70	10	0.75[h]	3.89	1.4	1.0	2.1[e]	1.9[e]	84	82
11	**6**	2-Me-THF	50	10	1.75[h]	5.54	2.0	1.2	1.7[d]	5.2[d]	54	97
12	**6**	2-Me-THF	70	10	0.5[h]	1.93	0.7	0.9	1.3[d]	4.3[d]	67	94
13	**7**	2-Me-THF	50	10	1.25[h]	3.24	1.2	1.0	1.5[e]	1.7[e]	83	81
14	**7**	2-Me-THF	70	10	1.0	0.34	0.1	0.8	2.2[e]	1.4[e]	80	85

Polymerization conditions: 40 bar C_2H_4, 100 mL solvent. [a] No product obtained. [b] 10^4 *x* mol $[C_2H_4]$ *x* mol^{-1}[Ni]. [c] From ^1H NMR; determined by comparing the olefinic resonances to the backbone resonance intensity. [d] Determined by gel permeation chromatography (GPC) at 160 °C in dichlorobenzene, universal calibration (with polystyrene). [e] Determined by GPC at 50° C in THF, linear calibration against PS. [f] Branches per 1000 C atoms. [g] Determined by $^{13}C\{^1H\}$ NMR (inverse gated), for detailed microstructure analysis see Supporting Information. [h] Polymerization run until ethylene uptake ceased.

es S43—S47 for ethylene uptake over time. Note these experiments were run until complete deactivation of the catalyst, to probe for stability).

The impact of the cyclophane structure on catalysis was elucidated by density function theory (DFT) methods. Conformational analysis showed, that the conformers with the non-coordinated imine rotated away are about 3 kcal mol^{-1} more stable compared to the conformers with the imine rotated towards the nickel atom, due to a lower steric pressure of the terphenyl group on the second imine, and an attractive imine–CH···O interaction. Therefore, the most sterically hindered area is in the left hemisphere of topographic steric maps[22] (Figure 3). Notably, the cyclophane structure also introduces steric pressure in the apical positions and in the right hemisphere.

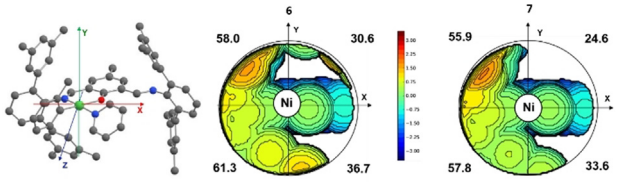

Figure 3. Topographic steric maps and %VBur divided by quadrants of **6** (center) and **7** (right). The complexes are oriented as shown for **7** on the left. Distance in the color scale is in Å.

The cyclophanes' rigidity increases energies for intermediates and transition states with a high steric demand, while the additional imine donor does not affect catalysis as elucidated by a full DFT study of all relevant pathways. Modelling starts with **1-β-T**, a complex with a β-agostic interaction and the growing alkyl chain *trans* to the oxygen atom (referenced as the zero point energy, Scheme 3). The first step is an ethylene coordination to **2-Coor-T**, followed by isomerization to **2-Coor-C**. The energies for the intermediates and the rate determining step for this process are similar for both systems (**6** and **7**), and do not differ from mono-(imino)phenoxy catalysts.[13]

Starting from **2-Coor-C**, either chain propagation (ethylene insertion to **2-β-T**) or branch formation and chain transfer (through ethylene de-coordination and BHE to **1-BHE-C**) are possible. Ethylene insertion via **TS-2$_{ins}$** to **2-β-T** is attributed with similar energies for both systems (**6** and **7**). The entire ethylene insertion process is not influenced by the C4 bridges or the non-coordinating imine donor.

The energy barriers associated with BHE (overall: going from **2-Coor-C** via **1-β-C** to **1-BHE-C**) are similar for the cyclophane and reference catalyst. In detail, ethylene de-coordination from **2-Coor-C** to **1-β-C** can proceed either directly via **TS-2$_{decoor}$**, or in a two-step pathway as assisted ethylene de-coordination with a Ni-aryl complex (**1-Pr-C**) as an intermediate (a typical process for electron-rich mono-(imino)phenoxy catalysts[13]). For complex **7**, the two-step

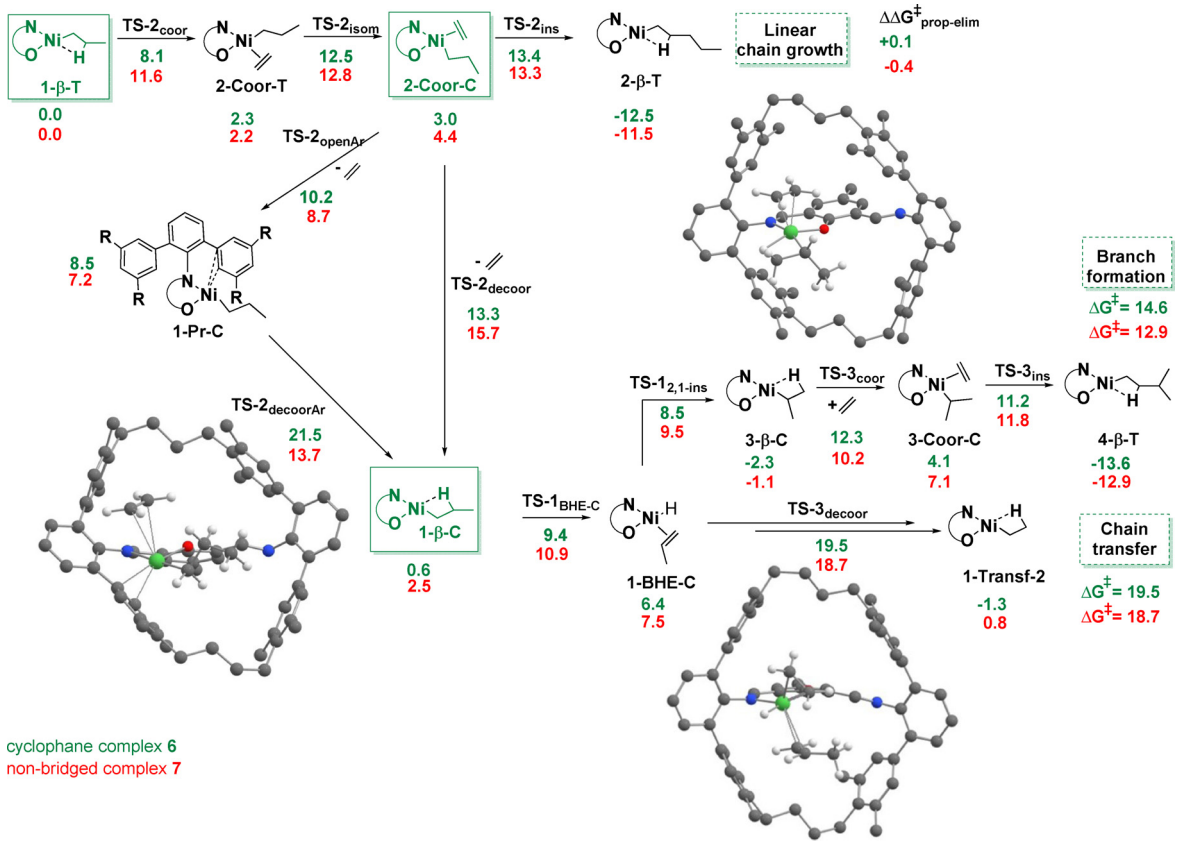

Scheme 3. Gibbs free energies (Δ*G* Tol in kcal mol^{-1}) of key species for linear chain growth, chain transfer and branch formation with **6** (green) and **7** (red). Optimized geometries of **TS-2$_{decoorAr}$**, **TS-3$_{decoor}$** and for **TS-3$_{coor}$** for **6** are shown.

pathway is 2.0 kcal mol^{-1} lower in energy compared to the direct pathway. For the cyclophane complex, the transition state to reach **1-Pr-C** via **TS-2**$_{\mathbf{decoorAr}}$ is very high in energy (21.5 kcal mol^{-1}) due to a high steric pressure between the rigid terphenyl group and the released ethylene. The direct ethylene de-coordination via **TS-2**$_{\mathbf{decoor}}$ is significantly lower in energy (13.3 kcal mol^{-1}) and thus preferred for complex **6**. The energy barriers for ethylene de-coordination, are comparable for both catalyst systems, despite the different pathways. The energy barriers for the next step yielding **1-BHE-C** are similar for both systems.

The rigid cyclophane ligand impedes branch formation. This pathway starts with the formation of a β-agostic complex **3-β-C** via **TS-1**$_{\mathbf{2,1\text{-}ins}}$ followed by ethylene coordination via **TS-3**$_{\mathbf{coor}}$ yielding **3-Coor-C**. Then, ethylene is inserted via **TS-3**$_{\mathbf{ins}}$ to give **4-β-T**. Here, the energy barrier for the cyclophane **6** (14.6 kcal mol^{-1}, see difference from **3-β-C** to **TS-3**$_{\mathbf{coor}}$) is 1.7 kcal mol^{-1} higher compared to the not-bridged catalyst **7** (12.9 kcal mol^{-1}, see difference from **3-β-C** to **TS-3**$_{\mathbf{ins}}$), explaining the lower branching density of the products obtained by **6** in the experimental studies.

The rate determining step of the chain transfer pathway (which occurs via two steps consisting of monomer coordination followed by chain de-coordination, for details see Supporting Information) is sterically demanding and, again, higher in energy for the cyclophane complex (19.5 kcal mol^{-1} for **6** vs. 18.7 kcal mol^{-1} for **7**). The ethylene molecule and the leaving propyl group are close to the left terphenyl group, which cannot rotate away due to the C4 bridges. Ultimately, the energy barriers for this transition state can account for the higher molecular weights obtained with **6** when compared to **7**, as chain transfer becomes slightly less favored compared to ethylene insertion ($\Delta\Delta G^{\neq}_{\text{transf-prop}} = 6.1$ kcal mol^{-1} for **6** and $\Delta\Delta G^{\neq}_{\text{transf-prop}} = 5.4$ kcal mol^{-1} for **7**).

We demonstrate how a cyclophane structure can be generated in square-planar complexes with two different chelating donors (*N,O*). The use of a second auxiliary imine function to ultimately connect the cyclophane to the chelating ligand enables utilization of a single type of aniline building block to construct the cyclophane. Experimental and theoretical studies of conformational structures and catalysis show this imine to be directed away from the active sites and inert, as anticipated. In the synthetic key step, a 30-membered cycle is formed by two concomitant ring closing metathesis events, followed by chemoselective hydrogenation. The cyclophane catalyst is more temperature stable and long-lived compared to a reference neutral Ni^{II} ethylene polymerization catalyst, particularly in polar solvents as a reaction medium. The distinct effect of the cyclophane motif on product molecular weight and branching microstructure can be traced to the increased energy of sterically demanding transition states. This affects the rate determining steps towards chain transfer and branch formation, while chain propagation remains highly effective.

Acknowledgements

Financial support by the DFG (Me 1388/14-1) is gratefully acknowledged. We thank Maximilian Baur and Steffen Iberl for their assistance as part of their undergraduate studies, Michael Linseis for assistance with single crystal analysis, Malin Bein for mass spectrometry measurements, Lars Bolk for DSC measurements and Manuel Schnitte and Florian Wimmer for GPC measurements. Open access funding enabled and organized by Projekt DEAL.

Keywords: cyclophanes · density functional calculations · ethylene polymerization · homogeneous catalysis · *N,O* ligands

[1] a) A. Nakamura, S. Ito, K. Nozaki, *Chem. Rev.* **2009**, *109*, 5215; b) Z. Chen, M. Brookhart, *Acc. Chem. Res.* **2018**, *51*, 1831; c) A. Keyes, H. E. Basbug Alhan, E. Ordonez, U. Ha, D. B. Beezer, H. Dau, Y.-S. Liu, E. Tsogtgerel, G. R. Jones, E. Harth, *Angew. Chem. Int. Ed.* **2019**, *58*, 12370; *Angew. Chem.* **2019**, *131*, 12498; d) D. J. Walsh, M. G. Hyatt, S. A. Miller, D. Guironnet, *ACS Catal.* **2019**, *9*, 11153; e) C. Tan, C. Chen, *Angew. Chem. Int. Ed.* **2019**, *58*, 7192; *Angew. Chem.* **2019**, *131*, 7268.

[2] a) M. Stürzel, S. Mihan, R. Mülhaupt, *Chem. Rev.* **2016**, *116*, 1398; b) G. Wilke, *Angew. Chem. Int. Ed.* **2003**, *42*, 5000; *Angew. Chem.* **2003**, *115*, 5150.

[3] a) L. K. Johnson, C. M. Killian, M. Brookhart, *J. Am. Chem. Soc.* **1995**, *117*, 6414; b) Z. Guan, P. M. Cotts, E. F. McCord, S. J. McLain, *Science* **1999**, *283*, 2059.

[4] D. H. Camacho, E. V. Salo, J. W. Ziller, Z. Guan, *Angew. Chem. Int. Ed.* **2004**, *43*, 1821; *Angew. Chem.* **2004**, *116*, 1857.

[5] D. H. Camacho, E. V. Salo, Z. Guan, *Org. Lett.* **2004**, *6*, 865.

[6] C. S. Popeney, Z. Guan, *J. Am. Chem. Soc.* **2009**, *131*, 12384.

[7] C. S. Popeney, D. H. Camacho, Z. Guan, *J. Am. Chem. Soc.* **2007**, *129*, 10062.

[8] D. H. Camacho, Z. Guan, *Chem. Commun.* **2010**, *46*, 7879.

[9] a) S. Mecking, M. Schnitte, *Acc. Chem. Res.* **2020**, *53*, 2738; b) M. Schnitte, A. Staiger, L. A. Casper, S. Mecking, *Nat. Commun.* **2019**, *10*, 2592; c) P. Kenyon, M. Wörner, S. Mecking, *J. Am. Chem. Soc.* **2018**, *140*, 6685; d) H. Mu, L. Pan, D. Song, Y. Li, *Chem. Rev.* **2015**, *115*, 12091; e) D. Takeuchi, Y. Chiba, S. Takano, K. Osakada, *Angew. Chem. Int. Ed.* **2013**, *52*, 12536; *Angew. Chem.* **2013**, *125*, 12768; f) M. R. Radlauer, A. K. Buckley, L. M. Henling, T. Agapie, *J. Am. Chem. Soc.* **2013**, *135*, 3784; g) Z. Chen, M. Mesgar, P. S. White, O. Daugulis, M. Brookhart, *ACS Catal.* **2015**, *5*, 631; h) Q. H. Tran, M. Brookhart, O. Daugulis, *J. Am. Chem. Soc.* **2020**, *142*, 7198.

[10] T. R. Younkin, E. F. Connor, J. I. Henderson, S. K. Friedrich, R. H. Grubbs, D. A. Bansleben, *Science* **2000**, *287*, 460.

[11] H.-C. Chiu, A. Koley, P. L. Dunn, R. J. Hue, I. A. Tonks, *Dalton Trans.* **2017**, *46*, 5513.

[12] a) L. Wang, W.-H. Sun, L. Han, Z. Li, Y. Hu, C. He, C. Yan, *J. Organomet. Chem.* **2002**, *650*, 59; b) K. Ohno, K. Arima, S. Tanaka, T. Yamagata, H. Tsurugi, K. Mashima, *Organometallics* **2009**, *28*, 3256.

[13] L. Falivene, T. Wiedemann, I. Göttker-Schnetmann, L. Caporaso, L. Cavallo, S. Mecking, *J. Am. Chem. Soc.* **2018**, *140*, 1305.

[14] P. W. Glunz, L. Mueller, D. L. Cheney, V. Ladziata, Y. Zou, N. R. Wurtz, A. Wei, P. C. Wong, R. R. Wexler, E. S. Priestley, *J. Med. Chem.* **2016**, *59*, 4007.

[15] Deposition Numbers 2068251, 2068252, 2068253, 2068254 contain the supplementary crystallographic data for this paper. These data are provided free of charge by the joint Cambridge Crystallographic Data Centre and Fachinformationszentrum

Karlsruhe Access Structures service www.ccdc.cam.ac.uk/structures.
[16] T. W. Greene, P. G. M. Wuts, *Protective Groups in Organic Synthesis* Wiley, New York, NY, **1999**.
[17] I. Göttker-Schnetmann, S. Mecking, *Organometallics* **2020**, *39*, 3433.
[18] C. Wang, S. Friedrich, T. R. Younkin, R. T. Li, R. H. Grubbs, D. A. Bansleben, M. W. Day, *Organometallics* **1998**, *17*, 3149.
[19] A. Bondi, *J. Phys. Chem.* **1964**, *68*, 441.
[20] T. Wiedemann, G. Voit, A. Tchernook, P. Roesle, I. Göttker-Schnetmann, S. Mecking, *J. Am. Chem. Soc.* **2014**, *136*, 2078.
[21] P. Wehrmann, M. Zuideveld, R. Thomann, S. Mecking, *Macromolecules* **2006**, *39*, 5995.
[22] L. Falivene, R. Credendino, A. Poater, A. Petta, L. Serra, R. Oliva, V. Scarano, L. Cavallo, *Organometallics* **2016**, *35*, 2286.

Manuscript received: April 20, 2021
Accepted manuscript online: May 26, 2021
Version of record online: July 21, 2021

